Supporting Information for

Role of Fe Doping on Local Structure and Electrical and Magnetic Properties of $PbTiO_3$

Hasitha Ganegoda,[†,=] Soham Mukherjee,[*,‡] Beihai Ma,[¶] Daniel T. Olive,[†,#] James H. McNeely,[§,@] James A. Kaduk,[§,∥] Jeff Terry,[†] Håkan Rensmo,[‡] and Carlo U. Segre[*,†]

[†] *Department of Physics & Center for Synchrotron Radiation Research and Instrumentation, Illinois Institute of Technology, Chicago, Illinois 60616, USA*

[‡] *Department of Physics and Astronomy Uppsala University, 752 36 Uppsala, Sweden*

[¶] *Applied Materials Division, Argonne National Laboratory, Argonne, Illinois 60439, United States*

[§] *Department of Chemistry, Illinois Institute of Technology, Chicago, Illinois 60616, United States*

[∥] *Poly Crystallography, Inc., Naperville, Illinois 60540, United States*

[=] *Present address: CTS Corporation, Lisle, Illinois 60532, United States*

[#] *Present address: Materials Science and Technology Division, Los Alamos National Laboratory, Los Alamos, New Mexico 87545, United States*

[@] *Present address: Department of Chemistry, Boston University, Boston, Massachusetts 02215, United States*

[*] *Corresponding authors: soham.mukherjee@physics.uu.se; segre@iit.edu*

Sample preparation

A. Polycrystalline $PbTi_{1-x}Fe_xO_3$

Our PTF samples were prepared using an acetic acid based sol–gel route. All reagents of choice, lead subacetate, Pb $(C_2H_3O_2)_2{\cdot}2Pb(OH)_2$ (Sigma-Aldrich, ACS reagent grade) iron(III) acetylacetonate, $Fe(C_5H_7O_2)_3$ (Sigma-Aldrich, 99.9%), and titanium isopropoxide $Ti(OCH(CH_3)_2)_4$ (Sigma-Aldrich 99.999%), have good solubility in the solvent, acetic acid (Thermo-Fisher 98.5%). Stoichiometric solutions with desired Fe-concentrations were prepared by dissolving appropriate amounts of precursor powders in acetic acid. Lead sub- acetate and iron(III) acetylacetonate powders were separately dissolved in small beakers using 25–35 ml of acetic acid. Complete dissolution was achieved with the aid of a magnetic stirrer. Excess amounts of lead (typically 3%) were used to compensate for possible lead volatilization. On complete dissolution, two solutions were poured into a large beaker and stirred for approximately 10 min. Subsequently, a stoichiometric amount of titanium isopropoxide, typically between 1.25 and 5 ml was added while the solution was constantly being stirred. The solution was ultrasonicated for 1–3 h where longer sonication times are associated with higher iron concentrations. The solution was then transferred into a Petri dish for gel formation. Drying was carried out inside a 75 °C furnace and dried samples were ground and pyrolyzed in air at 300 °C for 5 h. Samples were then re-ground and calcined in air at 700 °C for 3 h to form the crystallized powders.

B. $PbTi_{1-x}Fe_xO_3$ Thin films (x = 0.1, 0.2)

Two 0.5 M sol-gel precursor solutions with x = 0.1 and 0.2 compositions with 12% excess lead were prepared and aged for 2 days before depositing thin films. The films were deposited on a Si substrate with SiO_2 (500 nm), Ti (50 nm), and Pt (200 nm) overlayers. The substrate dimensions were $10 \times 10 \times 0.5$ mm^3 with a terminating platinum surface of roughness less than 5 Å. The substrate was mounted on the vacuum chuck of a spin coater (Laurell Technologies, WS-400). The substrate was cleaned using ethanol followed by blowing dry nitrogen The precursor solution was first filtered using a syringe and a 0.02 μm filter. A few drops of the filtered solution were placed on the substrate and spin coated at 3000 rpm for 30 seconds. The freshly coated sample with a light green color was subsequently dried inside a 125 °C furnace for 5 to 10 minutes. The completely dried sample was first placed inside an alumina combustion boat then inserted into a 1 inch diameter tube furnace and heated to 300 ≯C. After 5 minutes of firing the sample was removed from the furnace and allowed to cool down to room temperature. Preliminary firing changed the sample color from light green to bright purple. After cleaning the sample surface with ethanol and dry nitrogen, it was placed inside a furnace heated to 650 °C and annealed for 3 minutes. The color of the film after this step was bright golden. Lead lanthanum zirconate titanate samples prepared using 0.5 M solutions under similar conditions were bright golden at a film thickness of approximately 115 nm and deep golden at approximately 120 nm. Films with thickness greater than 120 nm were red or green in color. Therefore, it is reasonable to assume that a single layer of our sample is approximately 115 nm in thickness. An additional 2 layers (total of 3 layers, approximately 345 nm) were deposited using the procedure described above. To improve the film quality and homogeneity, the final annealing step was carried out for total of 6 minutes. Both samples (x = 0.1 and 0.2) were investigated using XRD and found to have diffraction patterns similar to the powder samples, which were free from any impurity phases. Thin films were then prepared for dielectric measurements by depositing 250 μm diameter Pt electrodes on the surface.

Magnetic measurements

Magnetic measurements of the powder samples were carried out using a Quantum Design PPMS 6000 extraction magnetometer. A small amount of sample powders typically 20–240 mg was placed inside a Teflon capsule and secured using an end cap. The design of the end cap prevents any relative motion of the powder against the Teflon capsule during measurements. Pellet samples prepared in this study were not compatible with the magnetometer design due to their large diameter and the phase segregation that is found to occur after high temperature sintering. Consequently, magnetic measurements were limited to powder samples.

Ti K-edge EXAFS fitting

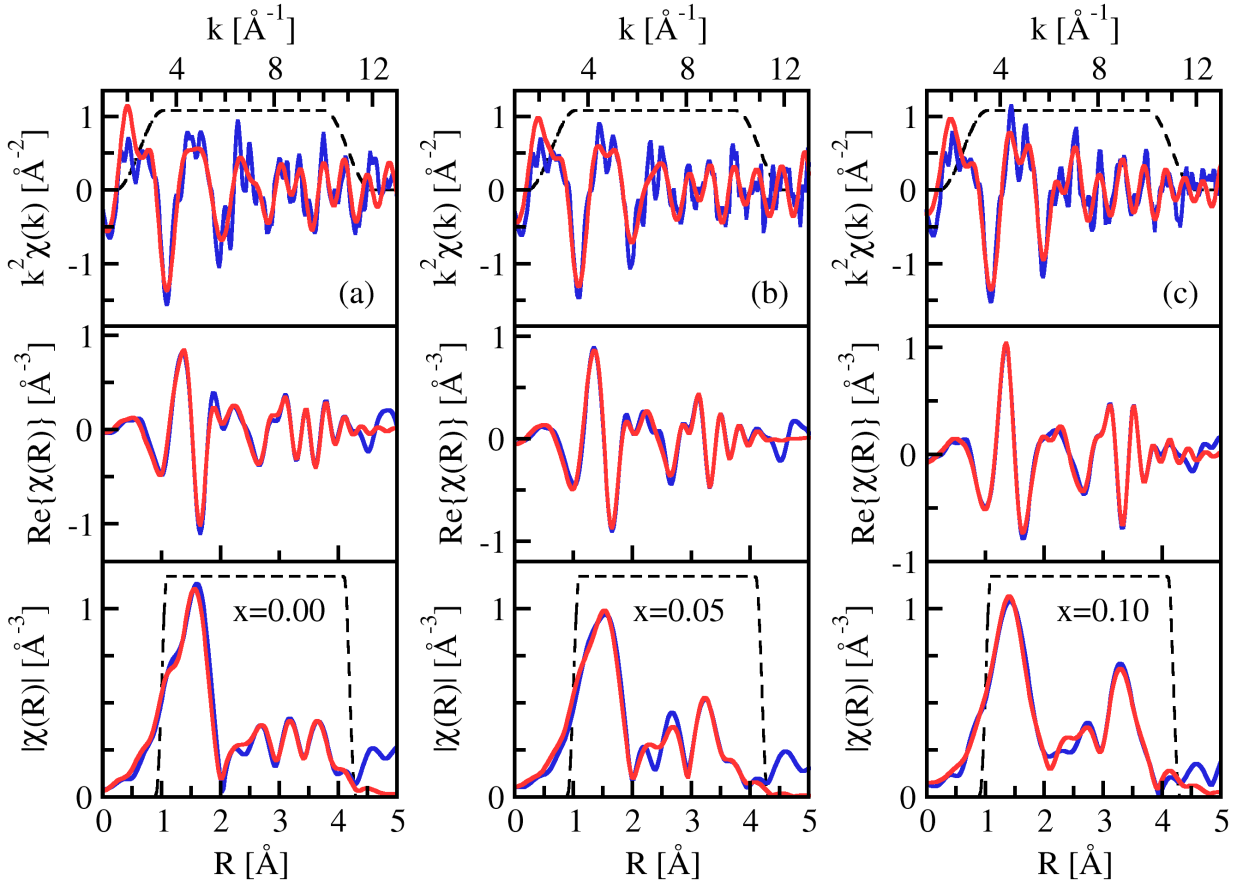

Figure S1a. Ti-K EXAFS data (in blue) for $PbFe_xTi_{1-x}O_3$ systems: (a) $x = 0.00$, (b) $x = 0.05$ and (c) $x = 0.1$ and their corresponding fits (in red) plotted in k^2-weighted $\chi(k)$ (upper panel), real part of $\chi(R)$ (middle panel) and modulus of the $\chi(R)$ functions (bottom panel). The fitting ranges are marked with Hanning window functions (in black dashed lines) having widths $\Delta k = 2.0$ Å^{-1} and $\Delta R = 0.2$ Å.

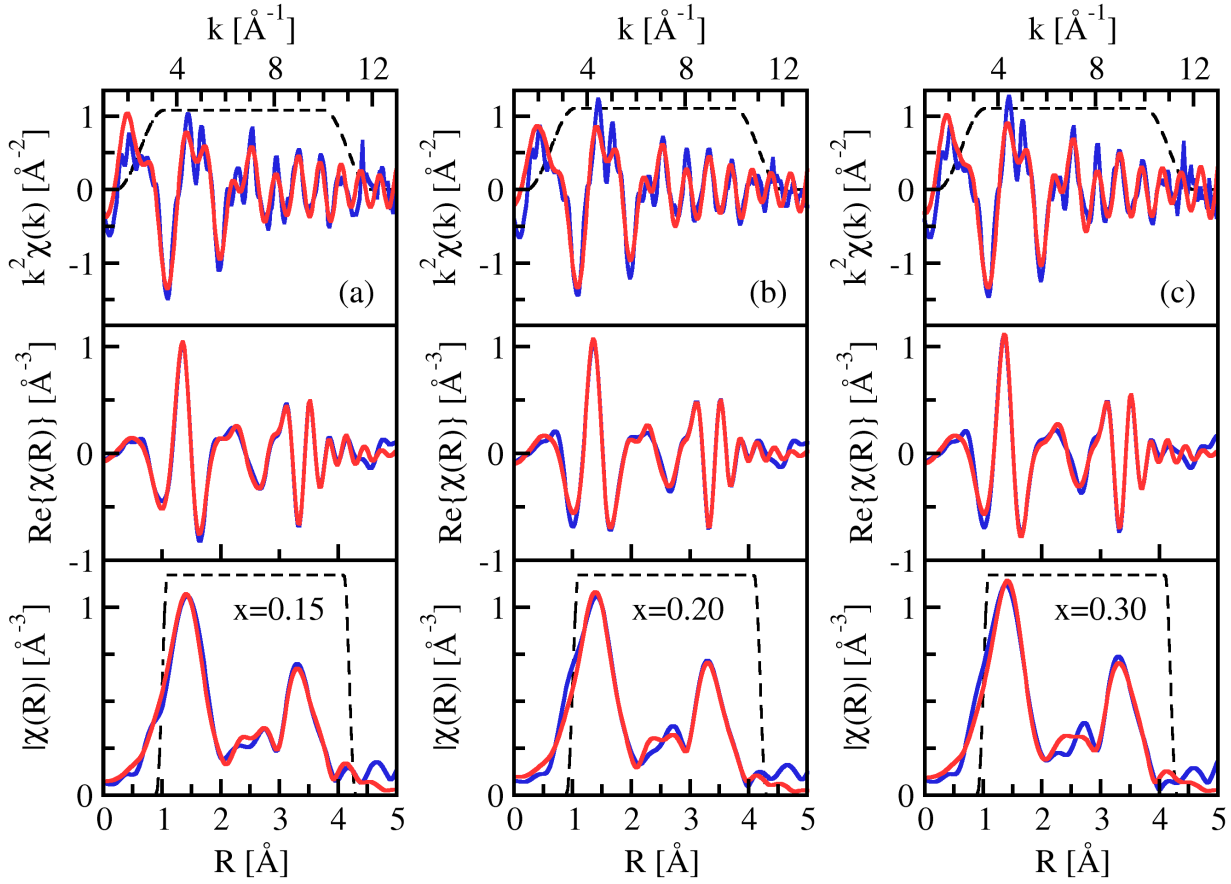

Figure S1b. Ti-K EXAFS data (in blue) for $PbFe_xTi_{1-x}O_3$ systems: (a) $x = 0.15$, (b) $x = 0.2$ and (c) $x = 0.3$ and their corresponding fits (in red) plotted in k^2-weighted $\chi(k)$ (upper panel), real part of $\chi(R)$ (middle panel) and modulus of the $\chi(R)$ functions (bottom panel). The fitting ranges are marked with Hanning window functions (in black dashed lines) having widths $\Delta k = 2.0$ Å^{-1} and $\Delta R = 0.2$ Å.

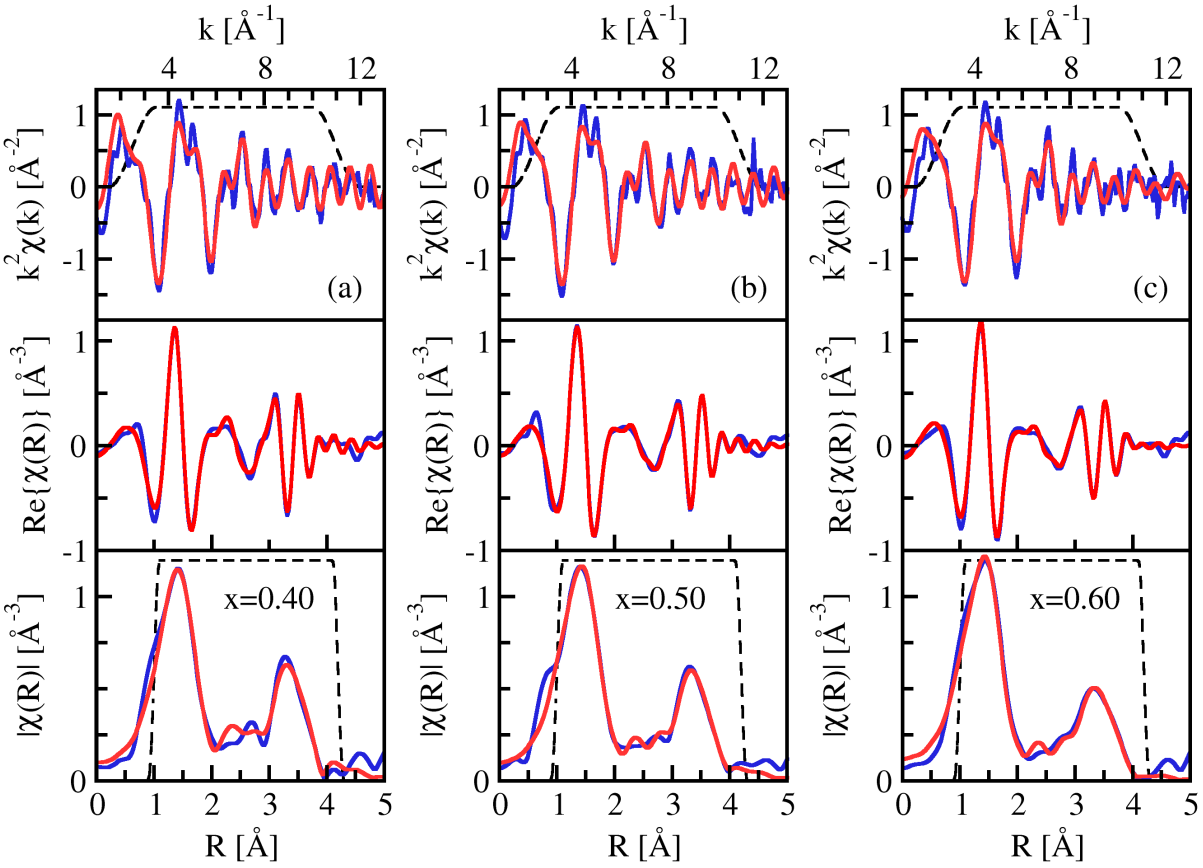

Figure S1c. Ti-K EXAFS data (in blue) for $PbFe_xTi_{1-x}O_3$ systems: (a) x = 0.4, (b) x = 0.5 and (c) x = 0.6 and their corresponding fits (in red) plotted in k^2-weighted $\chi(k)$ (upper panel), real part of $\chi(R)$ (middle panel) and modulus of the $\chi(R)$ functions (bottom panel). The fitting ranges are marked with Hanning window functions (in black dashed lines) having widths Δk = 2.0 Å^{-1} and ΔR = 0.2 Å.

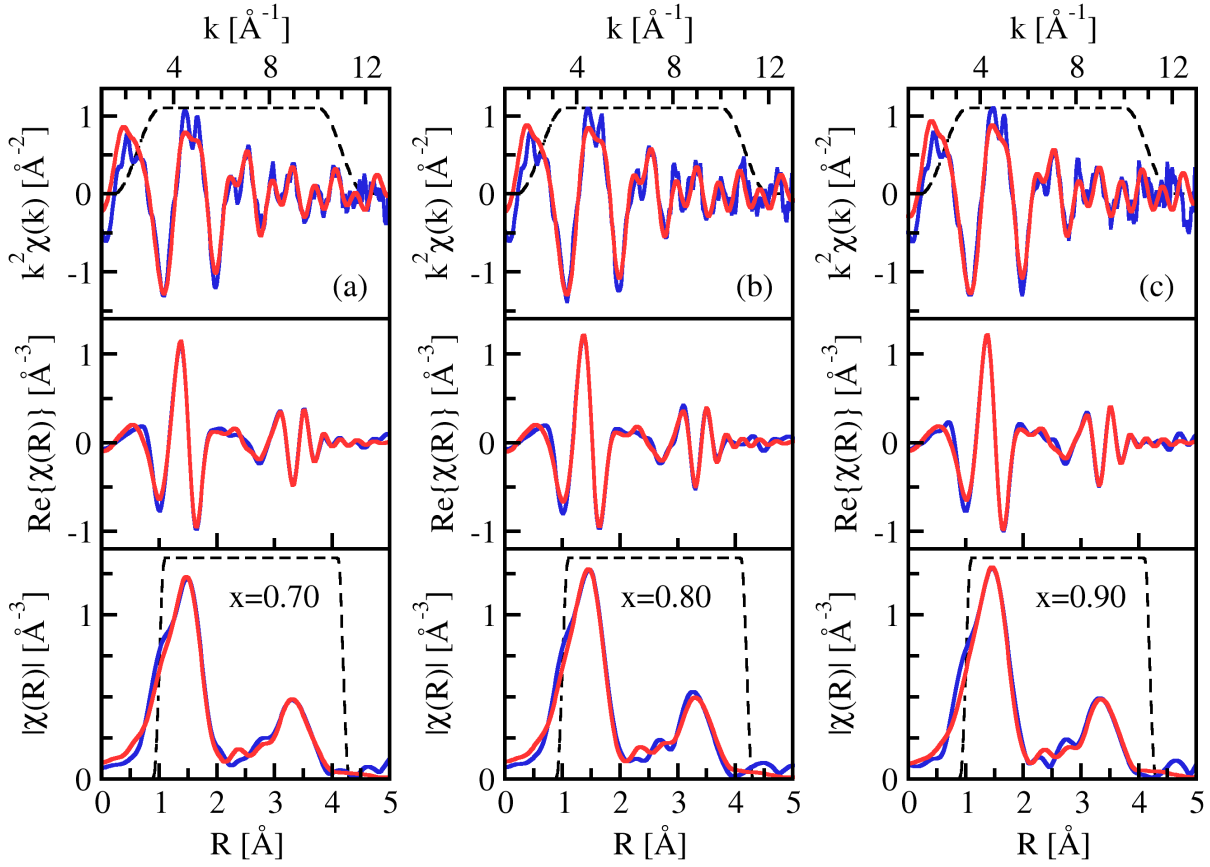

Figure S1d. Ti-K EXAFS data (in blue) for $PbFe_xTi_{1-x}O_3$ systems: (a) $x = 0.7$, (b) $x = 0.8$ and (c) $x = 0.9$ and their corresponding fits (in red) plotted in k^2-weighted $\chi(k)$ (upper panel), real part of $\chi(R)$ (middle panel) and modulus of the $\chi(R)$ functions (bottom panel). The fitting ranges are marked with Hanning window functions (in black dashed lines) having widths $\Delta k = 2.0$ Å^{-1} and $\Delta R = 0.2$ Å.

Table S1. Ti-K EXAFS first shell fits: bond lengths for shorter axial Ti-O [$R(\text{Ti-O})_{\text{short}}$], longer axial [$R(\text{Ti-O})_{\text{long}}$], and equatorial Ti-O [$R(\text{Ti-O})_{\text{ab}}$] bonds, corresponding σ^2 values and quality of the fit.

x	$R(\text{Ti-O})_{\text{short}}$	$R(\text{Ti-O})_{\text{long}}$	$\sigma^2(\text{Ti-O})$	$R(\text{Ti-O})_{\text{ab}}$	$\sigma^2(\text{Ti-O})_{\text{ab}}$	R-factor
0.0	1.732±0.019	2.388±0.03	0.0015	1.919±0.01	0.0050±0.0009	1.8%
0.005	1.74±0.02	2.38±0.027	0.002	1.926±0.011	0.0058±0.0009	2.4%
0.01	1.742±0.02	2.378±0.033	0.0025	1.925±0.01	0.0054±0.0007	3.9%
0.05	1.759±0.041	2.377±0.058	0.003	1.926±0.019	0.0068±0.0024	1.8%
0.075	1.779±0.061	2.396±0.077	0.0111±0.009	1.913±0.016	0.0090±0.0028	2.5%
0.1	1.792±0.057	2.424±0.09	0.009	1.913±0.015	0.0096±0.0033	1.4%
0.125	1.784±0.068	2.436±0.083	0.0112±0.0101	1.914±0.018	0.0098±0.0031	2.0%
0.15	1.817±0.052	2.404±0.039	0.0079±0.0049	1.917±0.014	0.0101±0.0027	1.8%
0.2	1.858±0.107	2.444±0.036	0.0080±0.0045	1.918±0.025	0.0124±0.0055	1.0%
0.3	1.850±0.058	2.421±0.026	0.0063±0.0028	1.921±0.014	0.0111±0.0034	1.3%
0.4	1.825±0.058	2.444±0.057	0.0070±0.0062	1.918±0.017	0.0094±0.0032	0.8%
0.5	1.807±0.044	2.441±0.039	0.0064±0.0039	1.917±0.011	0.0087±0.0024	0.5%
0.6	1.797±0.041	2.446±0.047	0.0037±0.0036	1.921±0.012	0.0067±0.0026	1.2%
0.7	1.772±0.036	2.44±0.05	0.0043±0.0039	1.919±0.012	0.0053±0.0019	1.0%
0.8	1.794±0.045	2.427±0.061	0.004	1.92±0.013	0.0057±0.0023	0.8%
0.9	1.788±0.037	2.435±0.052	0.003	1.924±0.013	0.0053±0.0019	0.5%

Table S2. Ti-K EXAFS higher neighboring shell fits: shorter equatorial Ti-Pb [$R(\text{Ti-Pb})_{\text{short}}$], longer axial [$R(\text{Ti-Pb})_{\text{long}}$] and Ti-$M$ (M = Ti/Fe) [$R(\text{Ti-}M)$] interatomic distances, corresponding σ^2 values and quality of the fit.

x	$R(\text{Ti-Pb})_{\text{short}}$	$R(\text{Ti-Pb})_{\text{long}}$	$\sigma^2(\text{Ti-Pb})$	$R(\text{Ti-}M)_{\text{short}}$	$R(\text{Ti-}M)_{\text{long}}$	$\sigma^2(\text{Ti-}M)$	R-factor
0.0	3.382±0.023	3.577±0.023	0.0058±0.0028	3.981±0.016	4.232±0.016	0.0063±0.0021	1.8%
0.05	3.375±0.024	3.570±0.024	0.0031±0.0023	4.052±0.032	4.303±0.032	0.0064±0.0037	1.8%
0.1	3.346±0.032	3.541±0.032	0.0060±0.0039	4.048±0.014	4.299±0.014	0.00162±0.0016	1.4%
0.15	3.343±0.022	3.538±0.022	0.0078±0.0027	4.045±0.008	4.296±0.008	0.0012±0.0007	1.8%
0.2	3.343±0.014	3.538±0.014	0.0058±0.0016	4.041±0.007	4.292±0.007	0.0012±0.0007	1.0%
0.3	3.256±0.029	3.451±0.029	0.0131±0.0041	4.000±0.010	4.250±0.010	0.0018±0.0008	1.3%
0.4	3.249±0.053	3.444±0.053	0.017±0.010	3.994±0.016	4.245±0.016	0.0027±0.0014	0.8%
0.5	3.231±0.052	3.426±0.052	0.023±0.010	4.004±0.012	4.255±0.012	0.0039±0.0013	0.5%
0.6	3.214±0.073	3.408±0.073	0.023±0.015	4.002±0.018	4.253±0.018	0.0051±0.0022	1.2%
0.7	3.157±0.057	3.352±0.057	0.035±0.011	3.995±0.009	4.246±0.009	0.0053±0.0012	1.0%
0.8	3.176±0.103	3.371±0.103	0.044±0.021	3.983±0.012	4.234±0.012	0.0051±0.0014	0.8%
0.9	3.158±0.068	3.353±0.068	0.037±0.013	3.993±0.011	4.244±0.011	0.0053±0.0014	0.5%

Fe K-edge EXAFS fitting

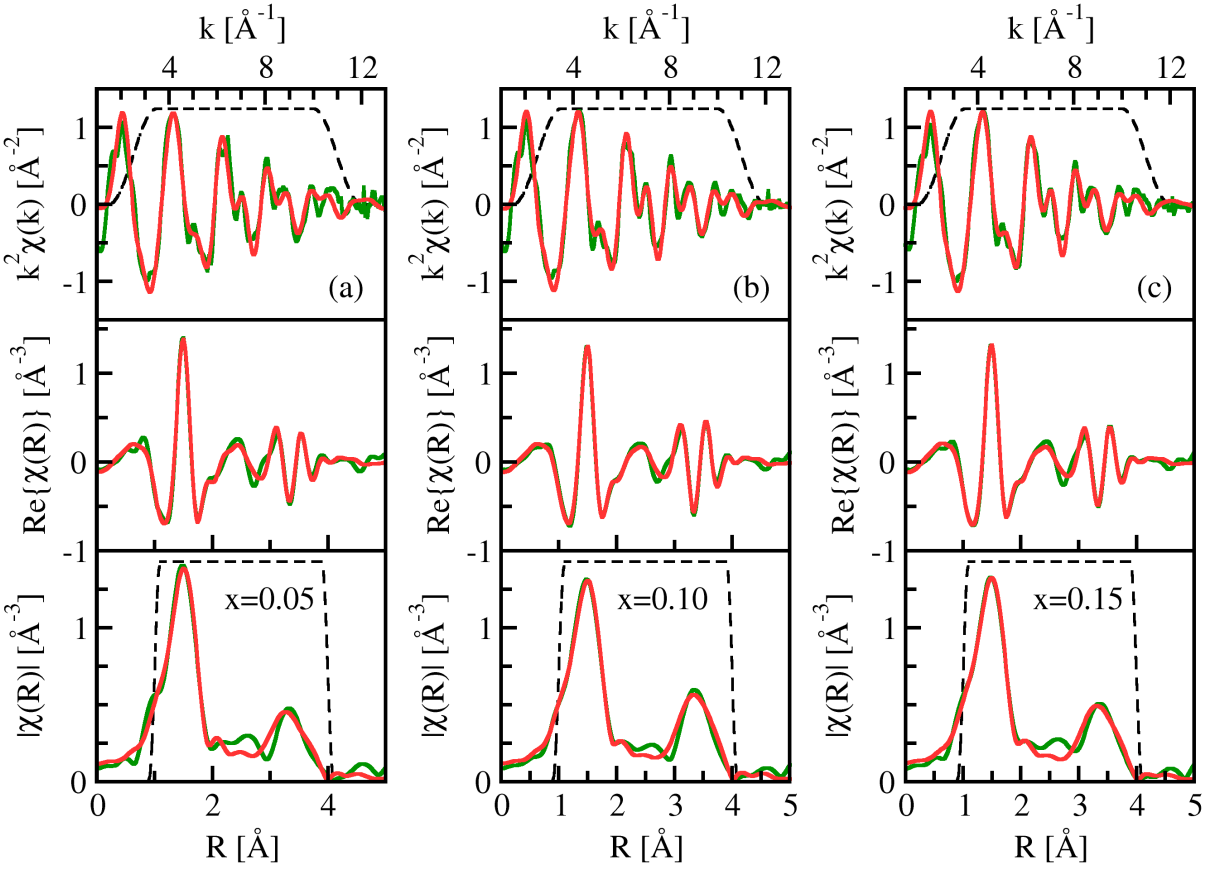

Figure S2a. Fe-K EXAFS data (in green) for $PbFe_xTi_{1-x}O_3$ systems: (a) x = 0.05, (b) x = 0.1 and (c) x = 0.15 and their corresponding fits (in red) plotted in k^2-weighted $\chi(k)$ (upper panel), real part of $\chi(R)$ (middle panel) and modulus of the $\chi(R)$ functions (bottom panel). The fitting ranges are marked with Hanning window functions (in black dashed lines) having widths Δk = 2.0 Å^{-1} and ΔR = 0.2 Å.

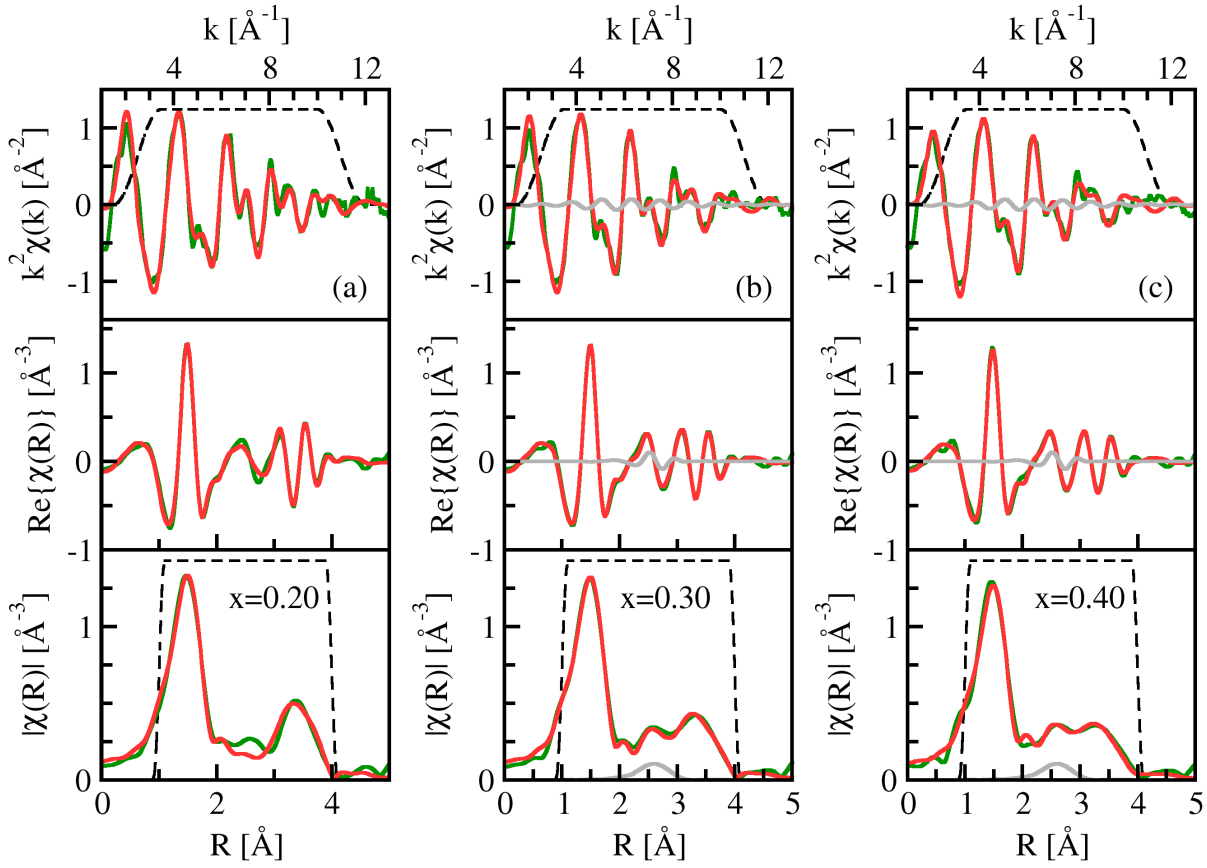

Figure S2b. Fe-K EXAFS data (in green) for $PbFe_xTi_{1-x}O_3$ systems: (a) x = 0.2, (b) x = 0.3 and (c) x = 0.4 and their corresponding fits (in red) plotted in k^2-weighted $\chi(k)$ (upper panel), real part of $\chi(R)$ (middle panel) and modulus of the $\chi(R)$ functions (bottom panel). The fitting ranges are marked with Hanning window functions (in black dashed lines) having widths Δk = 2.0 Å^{-1} and ΔR = 0.2 Å. Contribution of the short Fe-Fe correlations are presented in gray, detected for compositions $x \leq 0.3$.

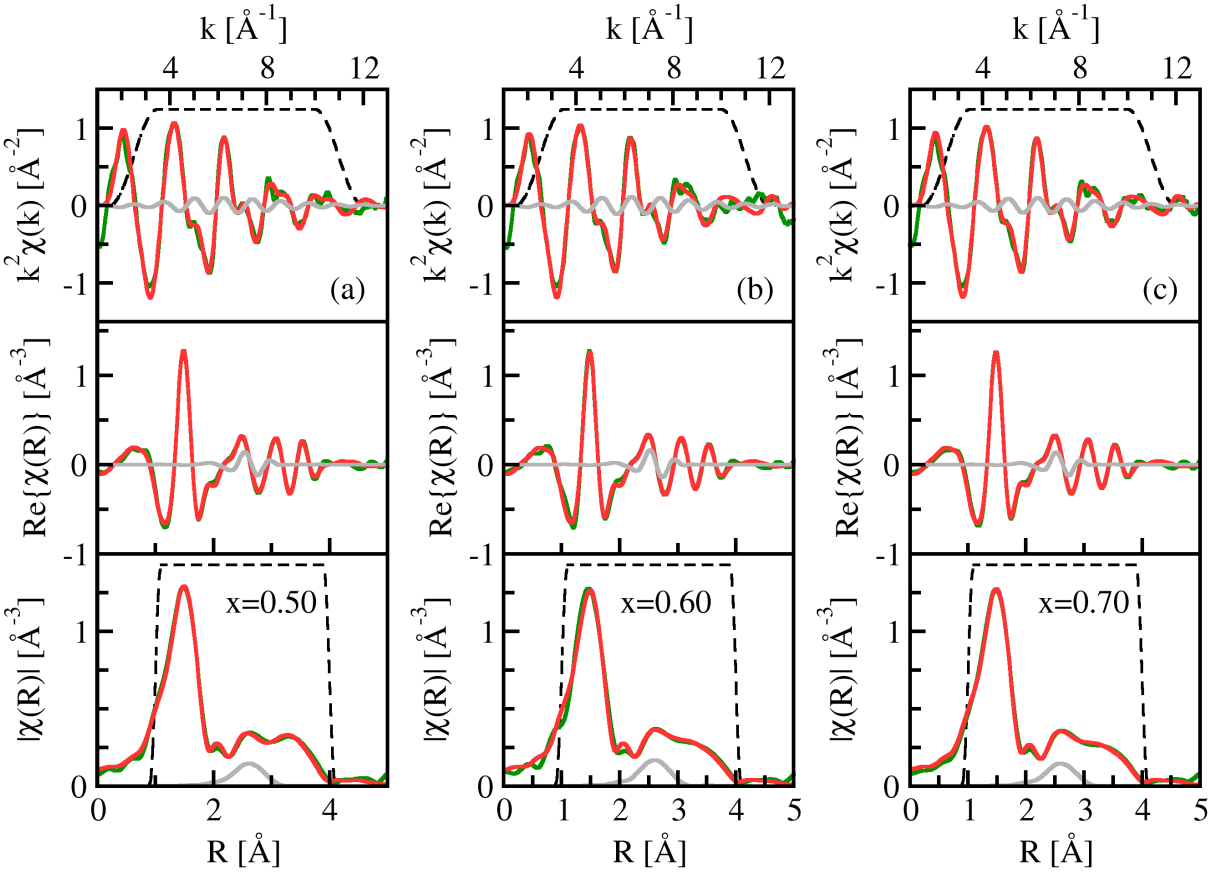

Figure S2c. Ti-K EXAFS data (in green) for $PbFe_xTi_{1-x}O_3$ systems: (a) x = 0.5, (b) x = 0.6 and (c) x = 0.7 and their corresponding fits (in red) plotted in k^2-weighted $\chi(k)$ (upper panel), real part of $\chi(R)$ (middle panel) and modulus of the $\chi(R)$ functions (bottom panel). The fitting ranges are marked with Hanning window functions (in black dashed lines) having widths Δk = 2.0 Å^{-1} and ΔR = 0.2 Å. Contribution of the short Fe-Fe correlations are presented in gray.

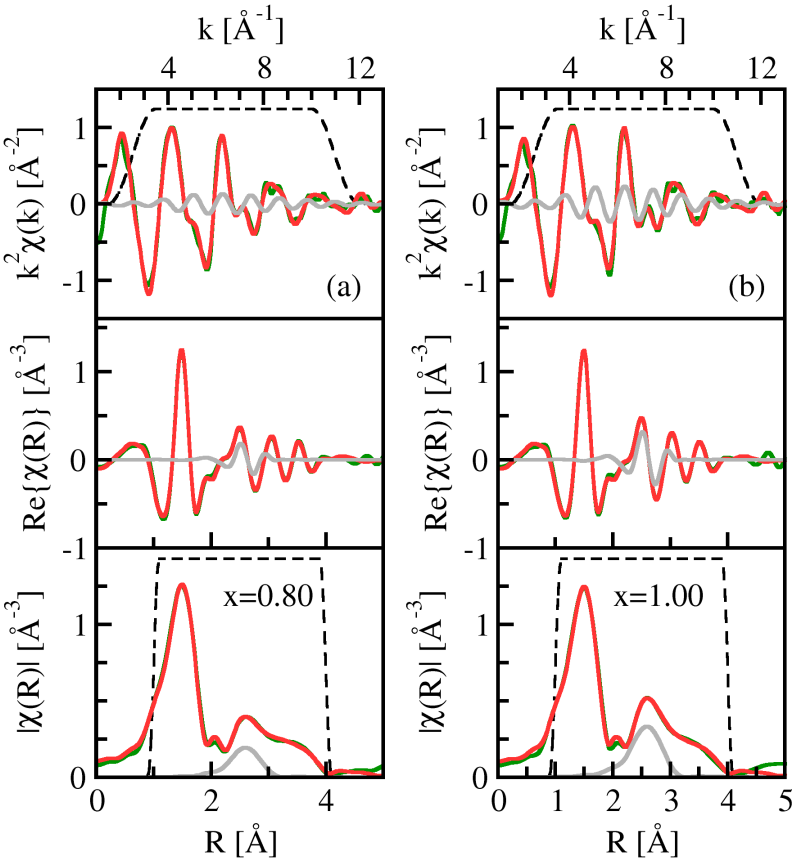

Figure S2d. Fe-K EXAFS data (in green) for $PbFe_xTi_{1-x}O_3$ systems: (a) x = 0.8 and (b) x = 1.0 and their corresponding fits (in red) plotted in k^2-weighted $\chi(k)$ (upper panel), real part of $\chi(R)$ (middle panel) and modulus of the $\chi(R)$ functions (bottom panel). The fitting ranges are marked with Hanning window functions (in black dashed lines) having widths Δk = 2.0 Å^{-1} and ΔR = 0.2 Å. Contribution of the short Fe-Fe correlations are presented in gray.

Table S3. Fe-K EXAFS first shell fits: coordination numbers ($N_{Fe\text{-}O}$), bond lengths ($R_{Fe\text{-}O}$), corresponding σ^2 values ($\sigma^2_{Fe\text{-}O}$), and quality of the fit.

x	$N_{Fe\text{-}O}$	$R_{Fe\text{-}O}$	$\sigma^2_{Fe\text{-}O}$	R-factor
0.05	5.01±0.81	1.984±0.015	0.0060±0.0024	2.2%
0.1	5.21±0.53	1.983±0.010	0.0073±0.0016	1.4%
0.15	5.30±0.43	1.980±0.008	0.0074±0.00013	1.2%
0.2	5.35±0.73	1.980±0.013	0.0074±0.0022	1.3%
0.3	5.17±0.40	1.977±0.009	0.0070±0.0011	0.6%
0.4	4.84±0.36	1.972±0.010	0.0070±0.0011	2.2%
0.5	4.76±0.33	1.973±0.007	0.0064±0.0011	0.5%
0.6	4.64±0.42	1.969±0.010	0.0064±0.0014	2.7%
0.7	4.63±0.32	1.970±0.007	0.0062±0.0010	0.5%
0.8	4.59±0.35	1.974±0.008	0.0062±0.0012	0.4%
1.0	4.60±0.62	1.976±0.006	0.0063±0.0008	0.3%

Table S4. Fe-K EXAFS higher neighboring shell fits: shorter equatorial Fe-Pb [$R(\text{Fe-Pb})_{short}$], longer axial [$R(\text{Fe-Pb})_{long}$], shorter equatorial Fe-*M* [$R(\text{Fe-}M)_{short}$] and longer axial Ti-*M* [$R(\text{Fe-}M)_{long}$] interatomic distances, corresponding σ^2 values and quality of the fit.

x	$R(\text{Fe-Pb})_{short}$	$R(\text{Fe-Pb})_{long}$	$\sigma^2(\text{Fe-Pb})$	$R(\text{Fe-}M)_{short}$	$R(\text{Fe-}M)_{long}$	$\sigma^2(\text{Fe-}M)$	R-factor
0.05	3.610±0.033	3.732±0.040	0.0070±0.0005	3.985±0.048	4.244±0.092	0.0160±0.0041	2.2%
0.1	3.624±0.021	3.753±0.023	0.0071±0.0005	3.945±0.021	4.268±0.039	0.0122±0.0021	1.4%
0.15	3.618±0.021	3.751±0.017	0.0071±0.0005	3.942±0.019	4.265±0.036	0.0139±0.00018	1.2%
0.2	3.619±0.028	3.756±0.032	0.0070±0.0005	3.945±0.028	4.274±0.055	0.0140±0.0033	1.3%
0.3	3.60±0.025	3.750±0.030	0.0074±0.0043	3.943±0.024	4.266±0.050	0.0161±0.0030	0.6%
0.4	3.574±0.027	3.713±0.028	0.0077±0.0046	3.890±0.014	4.121±0.075	0.0239±0.0089	2.2%
0.5	3.590±0.027	3.720±0.022	0.0081±0.0045	3.895±0.015	4.152±0.059	0.0228±0.0064	0.5%
0.6	3.567±0.024	3.719±0.025	0.0070±0.0010	3.890±0.016	4.130±0.079	0.0255±0.0092	2.7%
0.7	3.572±0.019	3.723±0.020	0.0070±0.0010	3.894±0.018	4.151±0.061	0.0243±0.0066	0.5%
0.8	3.571±0.022	3.726±0.024	0.0071±0.0010	3.887±0.019	4.145±0.070	0.0248±0.0074	0.4%
1.0	3.550±0.015	3.708±0.016	0.0070±0.0009	3.865±0.011	4.093±0.059	0.0281±0.0071	0.3%

Table S5. Fe-Fe correlations from $PbFe_{12}O_{19}$: EXAFS first shell fits: coordination numbers ($N_{Fe\text{-}Fe}$), bond lengths ($R_{Fe\text{-}Fe}$), corresponding σ^2 values ($\sigma^2_{Fe\text{-}Fe}$), and quality of the fit.

x	$N_{Fe\text{-}Fe}$	$R_{Fe\text{-}Fe}$	$\sigma^2_{Fe\text{-}Fe}$	R-factor
0.3	1.26±0.53	3.01±0.03	0.010±0.0008	0.6%
0.4	0.99±0.63	3.02±0.04	0.0099±0.0034	2.2%
0.5	1.10±0.54	3.04±0.02	0.0094±0.0033	0.5%
0.6	1.27±0.58	3.05±0.03	0.0099±0.0019	2.7%
0.7	1.29±0.47	3.05±0.02	0.0098±0.0019	0.5%
0.8	1.63±0.54	3.04±0.02	0.0099±0.0019	0.4%
1.0	2.64±0.72	3.03±0.01	0.0108±0.0025	0.3%